

# Asymmetry in Polymer-Solvent Interactions Yields Complex Thermoresponsive Behavior

Satyen Dhamankar and Michael A. Webb\*

*Department of Chemical and Biological Engineering, Princeton University, Princeton, NJ 08544*

(Dated: March 4, 2024)

Thermoresponsive polymers hold both fundamental and technological importance, but the essential physics driving their intriguing behavior is not wholly understood. We introduce a lattice framework that incorporates elements of Flory-Huggins solution theory and the  $q$ -state Potts model to study the phase behavior of polymer solutions and single-chain conformational characteristics. Importantly, the framework does not employ any temperature- or composition-dependent parameters. With this minimal Flory-Huggins-Potts framework, we show that orientation-dependent interactions, specifically between monomer segments and solvent particles, are alone sufficient to observe upper critical solution temperatures, miscibility loops, and hourglass-shaped spinodal curves. Signatures of emergent phase behavior are found in single-chain Monte Carlo simulations, which display heating- and cooling-induced coil-globule transitions linked to energy fluctuations. The model also capably describes a range of experimental systems. This work provides new insights regarding the microscopic physics that underpin complex thermoresponsive behavior in polymers.

Thermoresponsive polymers (TRPs) drastically alter structure, functionality, and/or stability upon changes in temperature.[1–3] They are appealing candidates for many applications, such as drug delivery, sensing, and purification.[4–12] Their physics also have implications for biological systems, with parallels to cold and warm denaturation of proteins, the hydrophobic effect, the formation of biomolecular condensates, and folding of DNA/RNA nanostructures.[13–22] Manipulating how polymer-based materials respond to temperature could also enhance control over supramolecular assemblies and improve particle engineering.[23–25] Consequently, understanding and modeling TRPs is of significant interest.

No self-contained theoretical framework currently captures the range of behaviors observed in TRPs. Flory-Huggins solution theory[26, 27] (FH) is a simple conceptual starting point, but balancing short-ranged interactions against chain and solvent entropy only yields upper critical solution temperatures (UCST) and heating-induced globule-coil transitions (GCT).[26–29] Emergence of lower critical solution temperatures (LCST) or heating-induced coil-globule transitions (CGT) has been addressed by theoretical extensions,[30–45] which either introduce adjustable parameters or impose *ad hoc* temperature-dependence to existing ones. Some representative strategies include utilizing void sites and instituting surface-area effect corrections[31], incorporating secondary lattices with temperature-dependent perturbative interactions[42, 44], invoking specific associative interactions,[46] or prescribing an equation of state.[34, 44, 45] Although these approaches are powerful and expressive, they often lack a firm microscopic basis, which inhibits validation, extension, interpretation, and application. By contrast, molecular simulation analysis has pointed to molecular size effects, hydrogen-bonding,

and other orientation-dependent interactions as important for thermoresponsive behavior.[16, 47–55] However, the chemical specificity obfuscates general comprehension and presents little opportunity to isolate the minimal and necessary set of interactions. Thus, questions remain regarding the microscopic physics of TRPs.

In this Letter, we introduce a minimal framework that combines elements of Flory-Huggins theory[26, 27] and the  $q$ -states Potts model[56, 57] to understand phase behavior and the CGT in TRPs. A key feature of this Flory-Huggins-Potts (FHP) framework is that all model parameters are linked to a Hamiltonian that transparently depends on pairwise interaction energies amongst monomer and solvent particles. By consequence, derived models are free of temperature- and composition-dependent parameters, permitting both analytical analysis and commensurate investigation with molecular simulation. Mean-field analysis reveals that asymmetry in monomer-solvent interactions is alone sufficient to produce intricate phase behavior, such as miscibility loops and hourglass-shaped phase envelopes, which are not captured by native FH. Furthermore, Monte Carlo simulations establish a connection between anticipated phase behavior and single-chain conformational characteristics, which enables microscopic analysis that extends our mean-field understanding. The FHP framework is also shown to reproduce diverse phase-coexistence data for several experimental systems. These findings not only highlight energetic asymmetries as important physics underlying TRPs but also establish a self-contained, conceptual framework that may be broadly applied to TRPs or extended to other stimuli-responsive systems.

We consider a lattice completely occupied by either solvent particles or monomer segments (Fig. 1a). Like FH, short-ranged, pairwise interactions exist between particles, and polymers consist of bonded monomer segments. Like a  $q$ -state Potts model, particles possess orientations that can influence pairwise energies. The system energy

---

\* mawebb@princeton.edu

is generally

$$\mathcal{H} = \frac{1}{2} \sum_{i=1}^N \sum_{j \in \mathcal{N}(i)} \varepsilon(\alpha_i, \alpha_j, \hat{\sigma}_i, \hat{\sigma}_j) + \sum_{k=1}^m \sum_{l=1}^{M-1} V(\vec{r}_{l+1}^{(k)}, \vec{r}_l^{(k)}) \quad (1)$$

with

$$V(\vec{r}_{l+1}^{(k)}, \vec{r}_l^{(k)}) = \begin{cases} 0 & \text{if } |\vec{r}_{l+1}^{(k)} - \vec{r}_l^{(k)}| \in \mathcal{N}(\mathcal{O}) \\ \infty & \text{otherwise} \end{cases} \quad (2)$$

where  $\alpha_i$  denotes the species (monomer or solvent) and  $\hat{\sigma}_i$  denotes the unit-vector orientation of the particle occupying the  $i$ th lattice site;  $\varepsilon(\cdot)$  is a pairwise energy function of such variables;  $N$  is the total number of lattice sites;  $m$  is the number of polymer chains;  $M$  is the number of monomer segments per chain;  $\vec{r}_l^{(k)}$  is the position of the  $l$ th monomer segment in the  $k$ th polymer chain; and  $V(\cdot)$  is a potential function that ensures bonded monomer segments occupy neighboring positions on the lattice (their distance is in the neighborhood of the origin,  $\mathcal{N}(\mathcal{O})$ ). Eq. (1) is distinguished from FH by the influence of particle orientations on pairwise energies.

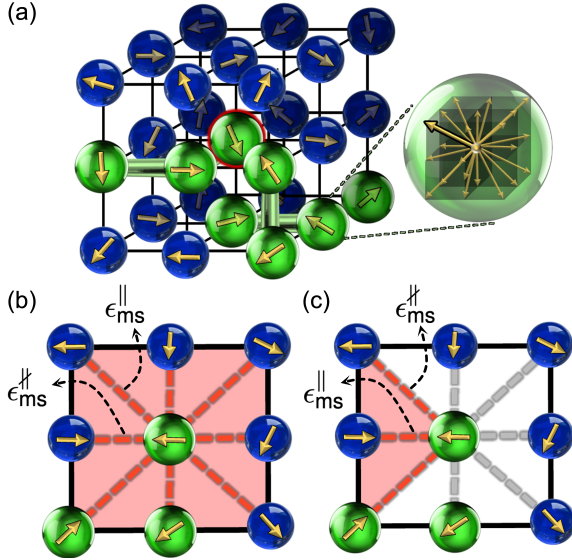


FIG. 1. Schematic of the Flory-Huggins-Potts framework. (a) The local neighborhood of a site (red outline) for a simple cubic lattice. Monomer (m) segments and bonds are in green, and solvent particles (s) are blue. (b, c) Two-dimensional illustrations of possible manifestations of orientation-dependent interactions. In (b), aligned interactions are permitted with all neighboring particles, which may capture physics akin to hydrogen-bond networks. In (c), aligned interactions are permitted with only a subset of neighboring particles, which may reflect specific and exclusive associative interactions. In both panels, particles adjoined by red lines in the shaded region can engage in aligned ( $\parallel$ ) interactions; those adjoined by gray only exhibit misaligned ( $\nparallel$ ) interactions.

To simplify, we decompose

$$\varepsilon(\alpha_i, \alpha_j, \hat{\sigma}_i, \hat{\sigma}_j) = \epsilon_{\alpha_i \alpha_j}^{\nparallel} + \Lambda(i, j) \Delta_{\alpha_i \alpha_j} \quad (3)$$

where  $\Delta_{\alpha_i \alpha_j} = \epsilon_{\alpha_i \alpha_j}^{\parallel} - \epsilon_{\alpha_i \alpha_j}^{\nparallel}$  is the difference between interaction energies for species  $\alpha_i$  and  $\alpha_j$  in an “aligned” ( $\parallel$ ) versus “misaligned” ( $\nparallel$ ) state, and  $\Lambda(i, j) \in [0, 1]$  functionally determines the extent to which particles at lattice sites  $i$  and  $j$  are aligned. By convention and without loss of generality, we presume  $\Delta_{\alpha_i \alpha_j} \leq 0$  such that aligned interactions are energetically favorable than misaligned. We envision that interaction asymmetries (i.e., differences in energy between aligned and misaligned states) arise from detailed chemical structure and molecular geometry. Two contrasting scenarios are depicted in Fig. 1b, which is inspired by hydrogen-bonding networks[58], and Fig. 1c, which is inspired by specific associative interactions[59, 60] (e.g., pi-pi stacking, metal–ligand, electrostatic). The primary distinction between these is the fraction of neighboring particles capable of aligned interactions, denoted  $p_v$  (red shading).

To gain insight into phase behavior, we consider the mean-field free energy. Following principles of FH and Boltzmann statistics (Supplemental Information, Section S1), the free energy of mixing per particle is

$$\frac{\Delta \bar{F}_{\text{mix}}}{k_B T} = \chi_{\text{FHP}}(T) \varphi(1 - \varphi) + \frac{\varphi}{M v_m} \ln \varphi + \frac{(1 - \varphi)}{v_s} \ln(1 - \varphi) \quad (4)$$

where  $\varphi$  is the volume fraction of the polymer,  $M$  is the degree of polymerization,  $v_m$  is the molar volume of a monomer segment, and  $v_s$  is the same for a solvent molecule (or group thereof). Furthermore,

$$\chi_{\text{FHP}}(T) \equiv \chi_{\text{FH}}(T) + \tilde{\chi}(T) \quad (5)$$

where

$$\chi_{\text{FH}}(T) \equiv \frac{(z - 2)}{k_B T} \left( \epsilon_{\text{ms}}^{\nparallel} - \frac{1}{2} \left( \epsilon_{\text{mm}}^{\nparallel} + \epsilon_{\text{ss}}^{\nparallel} \right) \right) \quad (6)$$

is essentially equivalent to a FH interaction parameter for a lattice with coordination number  $z$  and pairwise energies set at the misaligned energy scale, and

$$\tilde{\chi}(T) \equiv \frac{(z - 2)}{k_B T} p_v \left( \tilde{\Delta}_{\text{ms}}(T) - \frac{1}{2} \left( \tilde{\Delta}_{\text{mm}}(T) + \tilde{\Delta}_{\text{ss}}(T) \right) \right) \quad (7)$$

accounts for asymmetry between aligned and misaligned interactions and their relative prevalence. In particular, the  $\tilde{\Delta}_{ij}$  terms amount to per-site free-energy corrections between aligned and misaligned states given by

$$\tilde{\Delta}_{ij}(T) = \frac{\Delta_{ij}}{1 + r \exp(\Delta_{ij}/k_B T)} \quad (8)$$

where  $r = \frac{1-p_v}{p_v}$  is the fraction of possible misaligned to aligned microstates for a given pair of particles.

At this stage, we remark that FHP may appear deceptively complex. Eq. 4 itself is functionally analogous to the FH free energy of mixing, yet Eqs. (5)-(8) seemingly introduce five parameters beyond FH ( $\Delta_{\text{ms}}$ ,  $\Delta_{\text{ss}}$ ,  $\Delta_{\text{mm}}$ ,  $r$ , and  $p_v$ ) belying simplicity. However, neither

$p_v$  nor  $r$  are “free” parameters as they directly relate to the physical interactions (i.e., what constitutes aligned vs. misaligned) and follow from a defined Hamiltonian. This potentially leaves twice as many energy parameters compared to original FH. However, we will show that a minimal model to observe complex phase behavior only requires  $\Delta_{ms} < 0$  (with  $p_v$  and  $r$  as nonzero).

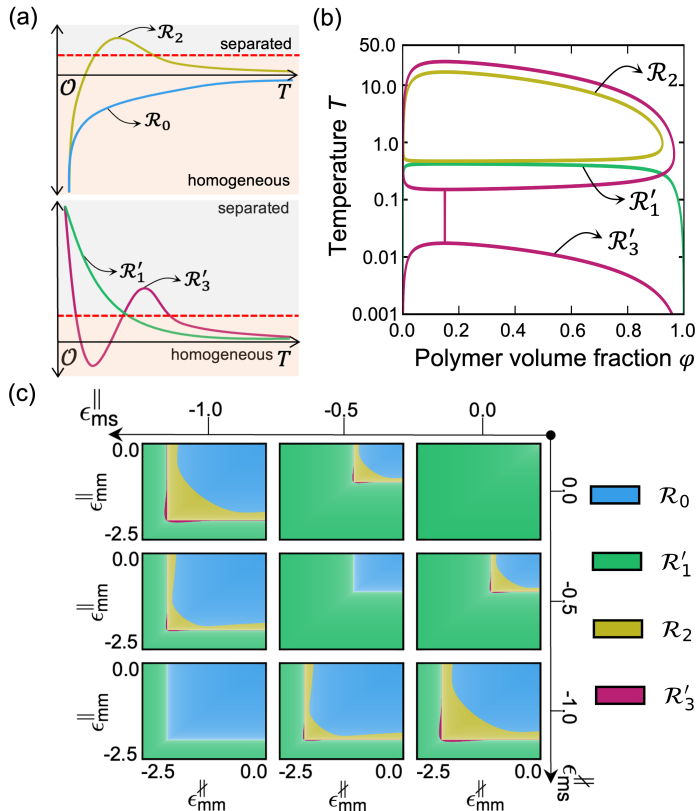


FIG. 2. Phase behavior of polymer solutions described by the Flory-Huggins-Potts framework. Representative temperature-volume fraction ( $T - \phi$ ) for a polymer with degree of polymerization  $M = 32$ , monomer molar volume  $v_m = 1$  and solvent molar volume  $v_s = 1$ . (a) Qualitative examples of  $\chi_{FHP}(T)$  for classification of phase behavior. Systems from  $\mathcal{R}_0$  are expected to be homogeneous, while those from  $\mathcal{R}'_1$ ,  $\mathcal{R}_2$ , and  $\mathcal{R}'_3$  respectively feature upper critical solution temperatures, miscibility loops, and hourglass-shaped phase envelopes. (b) Spinodal curves on temperature-volume fraction ( $T - \phi$ ) diagrams for models with parameters that yield  $\mathcal{R}'_1$ ,  $\mathcal{R}_2$ , and  $\mathcal{R}'_3$ ; parameters for  $\mathcal{R}_0$  yield only homogeneous phases. (c) Classification of phase behavior as a function of  $\epsilon_{mm}^{\parallel}$  and  $\epsilon_{mm}^{\parallel}$  (inner plots) at various values of  $\epsilon_{ms}^{\parallel}$  and  $\epsilon_{ms}^{\parallel}$  (outer axes). Results are obtained from mean-field analysis with  $(\epsilon_{ss}^{\parallel}, \epsilon_{ss}^{\parallel}, p_v, p_\Omega) = (0, 0, 1, 0.25)$  and  $z = 26$ . Additional parameter-sets are examined in Supplemental Information (Figs. S1, S2).

To illustrate, we characterize the phase behavior for a select set of models from four FHP-derived regimes. In FHP, we anticipate four regimes of qualitatively distinct  $\chi_{FHP}(T)$  behavior – denoted as  $\mathcal{R}_0$ ,  $\mathcal{R}'_1$ ,  $\mathcal{R}_2$ , or  $\mathcal{R}'_3$  (Fig. 2a) – that determine observed phases. The

notation is such that the subscript indicates the number of homogeneous-to-phase-separated transitions, a prime (') indicates a phase-separated state at low  $T$ , and no prime indicates a homogeneous state at low  $T$ . The spinodals in Fig. 2b illustrate how the FHP framework exhibits complex phase behavior relative to FH for specific parameter-sets representative of  $\mathcal{R}'_1$ ,  $\mathcal{R}_2$ , and  $\mathcal{R}'_3$ . While  $\mathcal{R}'_1$  displays UCST, which is well-captured in FH,  $\mathcal{R}_2$  and  $\mathcal{R}'_3$  respectively display a miscibility loop and an hourglass-like phase envelope, which is usually recovered by invoking an equation-of-state or otherwise presuming temperature-dependent parameters. Additionally, these models use  $\Delta_{mm} = \Delta_{ss} = 0$ , which suggests that the introducing interaction asymmetry to monomer-solvent interactions ( $\Delta_{ms} < 0$ ) is alone sufficient to obtain miscibility loops and hourglass-like phase envelopes.

Conversely, only introducing asymmetry to monomer-monomer interactions (or likewise solvent-solvent) does not result in as rich phase behavior. This is conveyed in Fig. 2c, which provides a “hyperphase diagram” summarizing  $\chi_{FHP}(T)$  behavior across a much broader parameter-space rather as opposed to the select cases in Fig. 2b. While the preponderance of parameter-space yields  $\mathcal{R}_0$  (blue) or  $\mathcal{R}'_1$  (green) behavior,  $\mathcal{R}_2$  (miscibility loops, yellow) and  $\mathcal{R}'_3$  (hourglass envelopes, magenta) emerge within intermediate energetic regimes only if misaligned and aligned monomer-solvent interactions are unequal. Overall, these results show how the balance of both homotypic and heterotypic interactions as well as misaligned and aligned interactions give rise to nuanced phase behavior, but asymmetric interactions between monomer and solvent are essential to observe multiple phase transitions within the FHP framework.

Because the parameters within FHP are traceable to a well-defined Hamiltonian, molecular simulation can be used to ascertain any connection between single-chain structure and solution thermodynamics (as established for FH[51, 61]). Monte Carlo (MC) simulations are used to characterize the temperature-dependent behavior of single polymer chains using parameters from each of  $\mathcal{R}_0$ ,  $\mathcal{R}'_1$ ,  $\mathcal{R}_2$ , and  $\mathcal{R}'_3$ . The simulations use  $M = 32$  and a  $\Lambda$  inspired by hydrogen-bonding networks

$$\Lambda_{\text{corr}}(i, j) = \Theta(\hat{\sigma}_i \cdot \hat{\sigma}_j - \delta), \quad (9)$$

which permits  $p_v = 1$  and for  $\delta = \cos 1$  gives  $r = 3$  (see also Fig. 1b). To probe single-chain conformations, we extract intra-chain scaling exponents  $\tilde{\nu}$  from

$$\langle |\vec{r}_i - \vec{r}_j|^2 \rangle \propto |i - j|^{2\tilde{\nu}} \quad (10)$$

and compare with known scaling laws (e.g.,  $R_g \propto M^{1/2}$  for ideal chains,  $R_g \propto M^{1/3}$  for globules).

Fig. 3a shows that distinct single-chain conformational behavior is observed when parameters are taken from different phase behavior regimes. At low  $T$ , systems from  $\mathcal{R}_0$  and  $\mathcal{R}_2$  exhibit scaling indicative of good-solvent conditions ( $\tilde{\nu} \geq 2/3$ ), while systems from  $\mathcal{R}'_1$  and  $\mathcal{R}'_3$  display more globular scaling; this correlates with  $\mathcal{R}_0$

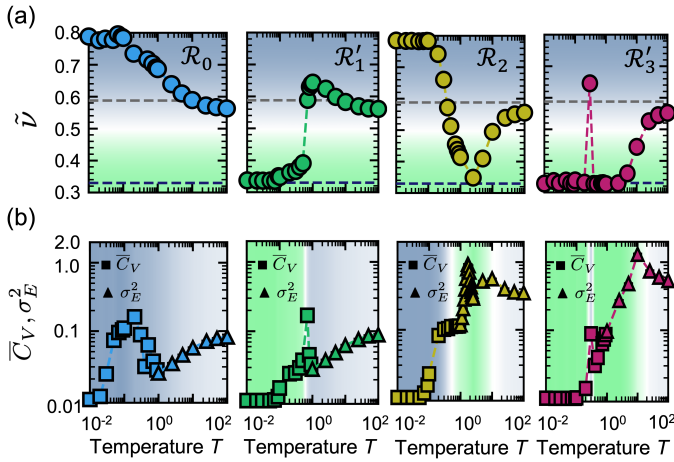


FIG. 3. Analysis of single-chain Monte Carlo simulations. (a,b) Temperature dependence of (a) intra-chain scaling exponent  $\tilde{\nu}$  and (b) energy fluctuations using parameters associated with  $\mathcal{R}_0$ ,  $\mathcal{R}'_1$ ,  $\mathcal{R}_2$  and  $\mathcal{R}'_3$ . In (a), the horizontal dashed lines are guides to the eye for globular scaling (black) and excluded-volume statistics (gray). In (b), the data transitions such that heat capacity  $\bar{C}_V$  is shown for  $T < 1.0$  and fluctuations in total energy  $\sigma_E^2$  is shown for  $T \geq 1.0$ ; the data are shifted by 0.01 to allow for logarithmic scaling. The background color is based on  $\tilde{\nu}$  to emphasize conformations that are expanded (blue) or globular (green) relative to the ideal chain (white). Error bars are smaller than the symbol size.

and  $\mathcal{R}_2$  having a single homogeneous phase and  $\mathcal{R}'_1$  and  $\mathcal{R}'_3$  featuring phase-separated states. Behavior between  $\mathcal{R}_0$  and  $\mathcal{R}_2$  differs upon heating. While  $\tilde{\nu}$  from  $\mathcal{R}_0$  gradually approaches excluded-volume statistics ( $\tilde{\nu} \sim 0.588$ ),  $\tilde{\nu}$  from  $\mathcal{R}_2$  collapses to a globule before expanding in the high- $T$  limit, which aligns with the physics of a miscibility loop. Similar explanations apply for  $\mathcal{R}'_1$  and  $\mathcal{R}'_3$ . The singular, sharp globule-coil transition for  $\tilde{\nu}$  from  $\mathcal{R}'_1$  with asymmetric monomer-monomer interactions is consistent with a UCST, but a sharp transition is only observed with sufficiently asymmetric interactions. For  $\mathcal{R}'_3$ ,  $\tilde{\nu}$  begins as globular then crosses the ideal-chain limit three times—a progression consistent with an hourglass-like phase envelope. In contrast,  $\tilde{\nu}$  obtained with FH only tends gradually and monotonically to excluded-volume statistics upon heating. Thus, anisotropic interactions can drive sharp, thermally induced conformational transitions – reminiscent of the trends seen in phase behavior.

The observed conformational transitions are also accompanied by drastic shifts in underlying energy fluctuations (Fig. 3b). For systems from  $\mathcal{R}'_1$ , the single CGT is marked by maxima in the heat capacity  $\bar{C}_V$  and energy fluctuations  $\sigma_E^2$  within a narrow temperature range wherein  $\tilde{\nu} \sim 0.5$  (white region); similar observations hold for the low- $T$  CGT in  $\mathcal{R}_2$  and  $\mathcal{R}'_3$ . In  $\mathcal{R}_2$  and  $\mathcal{R}'_3$ , a second higher- $T$  transition from globular to excluded-volume statistics is captured by a maximum in  $\sigma_E^2$ . These fluctuations notably accompany compositional and orientational changes within the polymer’s local environment

(Supplemental Information, Figs. S2 and S3) and are thus not reproducible by FH but are inherent to FHP.

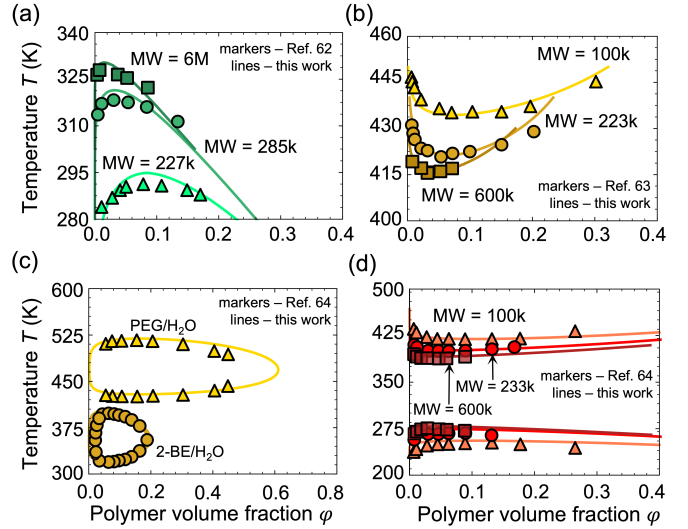


FIG. 4. Comparison to experimental coexistence data for diverse systems. Temperature-volume fraction ( $T-\phi$ ) diagrams for systems that display (a) upper critical solution temperatures, such as polyisobutylene (PIB) in diisobutyl ketone at several molecular weights (MW); (b) lower critical solution temperatures, such as polystyrene in ethyl acetate at several MW; (c) miscibility loops, such as polyethylene glycol (PEG) (3350 amu) in water and 2-butoxyethanol (2-BE) in water; and (d) hourglass-like phase behavior, such as polystyrene in tert-butyl acetate at several MW. The data in (a)-(d) are respectively sourced from Refs. [62], [63], and [64] and were also compared to theory proposed in Ref. [42, 65]. All molecular weights are reported in Daltons. All parameters are reported in the Supplemental Information (Table 4).

Finally, the FHP framework can quantitatively capture the behavior of experimental systems. This is illustrated in Fig. 4, which compares FHP results with experimental data for various solutions that collectively showcase UCST, LCST, miscibility loops, and hourglass (UCST + LCST) phase envelopes. These same systems were examined by Bae and Oh to evaluate a proposed double-lattice model.[63] Here, for each set of experimental data, the FHP parameters were optimized using the covariance matrix adaptation evolutionary strategy.[66] It is notable that FHP captures the experimental data well without any temperature-dependent parameters or externally imposed equation-of-state, which is distinct from similarly expressive prior theoretical works.[32, 44, 63] Although the quality of fits here does not firmly exclude the importance of other key interactions, the capacity to represent some facets of experimental data is not only an important demonstration for FHP but bolsters the case that energetic asymmetries, which distinguish FHP, are important to the physics of real systems.

In conclusion, we have introduced the Flory-Huggins-Potts (FHP) framework to describe and understand thermoresponsive polymers. Remarkably, this approach,

which simply extends Flory-Huggins (FH) theory with orientation-dependent interactions, showcases diverse temperature-dependent phase behavior, including miscibility loops and hourglass-like phase envelopes. In this way, FHP can capture the experimental data of diverse systems. This expressive capacity emerges without any *ad hoc* functional dependencies on temperature; the effects are transparently attributable to microscopic theory of interactions. Here, this enabled investigation of how polymer solution thermodynamics connect to single-chain conformational behavior. We find overall strong correspondence between single-chain conformational behavior (from molecular simulation) and macroscopic phase transitions (deduced from mean-field analysis), with multiple GCT transitions observed for a parameters that yield hourglass-like phase envelopes, for example. A key result from this analysis is that asymmetry in heterotypic (e.g., monomer-solvent) interactions is sufficient to induce complex thermoresponsive behavior, such as heating-induced CGT.

In the future, FHP can be extended and applied to other physical and chemical systems. Firstly, it can serve as foundational scaffolding to generate minimal models for other stimuli-responsive behaviors grounded in sim-

ilar physical principles. Secondly, the simplicity and transparency of FHP physics make it suitable for benchmarking and hypothesis testing in atomistic and coarse-grained simulation, and developing rigorous routines for bottom-up coarse-graining.[55, 67, 68] Thirdly, while the present work emphasizes fundamental conceptual physics and fitting to select experimental data, it is desirable to establish a connection or mapping between the physical framework of FHP with chemically realistic systems, such as phase-separating disordered proteins and RNAs.[69–71] Achieving quantitative consistency in some systems may require extensions to consider neglected factors, such as compressibility, which has been duly considered and effective elsewhere.

## ACKNOWLEDGMENTS

S.D. and M.A.W. acknowledge support from the National Science Foundation under Grant No. 2237470. Simulations were performed using resources from Princeton Research Computing at Princeton University, which is a consortium led by the Princeton Institute for Computational Science and Engineering (PICSciE) and Office of Information Technology’s Research Computing.

- 
- [1] M. Karimi, P. S. Zangabad, A. Ghasemi, M. Amiri, M. Bahrami, H. Malekzad, H. G. Asl, Z. Mahdieh, M. Bozorgomid, A. Ghasemi, M. R. R. T. Boyuk, and M. R. Hamblin, *ACS Applied Materials & Interfaces* **8**, 21107 (2016).
  - [2] Y.-J. Kim and Y. T. Matsunaga, *Journal of Materials Chemistry B* **5**, 4307 (2017).
  - [3] M. A. Ward and T. K. Georgiou, *Polymers* **3**, 1215 (2011).
  - [4] D. A. Davis, A. Hamilton, J. Yang, L. D. Cremar, D. V. Gough, S. L. Potisek, M. T. Ong, P. V. Braun, T. J. Martínez, S. R. White, J. S. Moore, and N. R. Sottos, *Nature* **459**, 68 (2009).
  - [5] Y. L. Colson and M. W. Grinstaff, *Advanced Materials* **24**, 3878 (2012).
  - [6] T. Tanaka, I. Nishio, S.-T. Sun, and S. Ueno-Nishio, *Science* **218**, 467 (1982).
  - [7] J. Thévenot, H. Oliveira, O. Sandre, and S. Lecommandoux, *Chemical Society Reviews* **42**, 7099 (2013).
  - [8] L. Zhai, *Chemical Society Reviews* **42**, 7148 (2013).
  - [9] D. Mukherji, M. D. Watson, S. Morsbach, M. Schmutz, M. Wagner, C. M. Marques, and K. Kremer, *Macromolecules* **52**, 3471 (2019).
  - [10] M. A. C. Stuart, W. T. S. Huck, J. Genzer, M. Müller, C. Ober, M. Stamm, G. B. Sukhorukov, I. Szleifer, V. V. Tsukruk, M. Urban, F. Winnik, S. Zauscher, I. Luzinov, and S. Minko, *Nature Materials* **9**, 101 (2010).
  - [11] D. Mukherji, C. M. Marques, and K. Kremer, *Annual Review of Condensed Matter Physics* **11**, 271 (2020).
  - [12] X. Xu, N. Bizmark, K. S. S. Christie, S. S. Datta, Z. J. Ren, and R. D. Priestley, *Macromolecules* **55**, 1894 (2022).
  - [13] X. Zeng, A. S. Holehouse, A. Chilkoti, T. Mittag, and R. V. Pappu, *Biophysical Journal* **119**, 402 (2020).
  - [14] J. S. Scarpa, D. D. Mueller, and I. M. Klotz, *Journal of the American Chemical Society* **89**, 6024 (1967).
  - [15] E. I. Shakhnovich and A. V. Finkelstein, *Biopolymers* **28**, 1667 (1989).
  - [16] P. de los Rios and G. Caldarelli, *Physical Review E* **62**, 8449 (2000).
  - [17] W. M. Gelbart, R. F. Bruinsma, P. A. Pincus, and V. A. Parsegian, *Physics Today* **53**, 38 (2000).
  - [18] Y. Shin and C. P. Brangwynne, *Science* **357** (2017), 10.1126/science.aaf4382.
  - [19] G. L. Dignon, W. Zheng, Y. C. Kim, and J. Mittal, *ACS Central Science* **5**, 821 (2019).
  - [20] C. Geary, P. W. K. Rothemund, and E. S. Andersen, *Science* **345**, 799 (2014).
  - [21] D. Han, X. Qi, C. Myhrvold, B. Wang, M. Dai, S. Jiang, M. Bates, Y. Liu, B. An, F. Zhang, H. Yan, and P. Yin, *Science* **358** (2017), 10.1126/science.aao2648.
  - [22] Y. Jia, L. Chen, J. Liu, W. Li, and H. Gu, *Chem* **7**, 959 (2021).
  - [23] J.-W. Yoo and S. Mitragotri, *Proceedings of the National Academy of Sciences* **107**, 11205 (2010).
  - [24] W. Lewandowski, M. Fruhnert, J. Mieczkowski, C. Rockstuhl, and E. Górecka, *Nature Communications* **6** (2015), 10.1038/ncomms7590.
  - [25] A. Bupathy, D. Frenkel, and S. Sastry, *Proceedings of the National Academy of Sciences* **119** (2022), 10.1073/pnas.2119315119.
  - [26] P. J. Flory, *The Journal of Chemical Physics* **17**, 303 (1949).
  - [27] P. J. Flory, *Principles of polymer chemistry* (Ithaca, NY,

Cornell University Press, 1953., 1953).

- [28] P. G. de Gennes, *Scaling Concepts in Polymer Physics* (Cornell University Press, 1979).
- [29] P. D. Gennes, *Journal de Physique Lettres* **36**, 55 (1975).
- [30] R. H. Lacombe and I. C. Sanchez, *The Journal of Physical Chemistry* **80**, 2568 (1976).
- [31] I. C. Sanchez and R. H. Lacombe, *The Journal of Physical Chemistry* **80**, 2352 (1976).
- [32] I. C. Sanchez and R. H. Lacombe, *Macromolecules* **11**, 1145 (1978).
- [33] C. G. Panayiotou, *Macromolecules* **20**, 861 (1987).
- [34] C. Panayiotou and I. C. Sanchez, *The Journal of Physical Chemistry* **95**, 10090 (1991).
- [35] B. A. Veytsman, *The Journal of Physical Chemistry* **94**, 8499 (1990).
- [36] D. S. Simmons and I. C. Sanchez, *Macromolecules* **41**, 5885 (2008).
- [37] D. S. Simmons and I. C. Sanchez, *Macromolecules* **43**, 1571 (2010).
- [38] R. Dahanayake and E. Dormidontova, *Physical Review Letters* **127**, 167801 (2021).
- [39] A. Matsuyama and F. Tanaka, *Physical Review Letters* **65**, 341 (1990).
- [40] S. Bekiranov, R. Bruinsma, and P. Pincus, *Physical Review E* **55**, 577 (1997).
- [41] J.-M. Choi, F. Dar, and R. V. Pappu, *PLOS Computational Biology* **15**, e1007028 (2019).
- [42] S. Y. Oh and Y. C. Bae, *Polymer* **49**, 4469 (2008).
- [43] Y. Hu, S. M. Lambert, D. S. Soane, and J. M. Prausnitz, *Macromolecules* **24**, 4356 (1991).
- [44] E. Clark and J. Lipson, *Polymer* **53**, 536 (2012).
- [45] G. R. Andersen and J. C. Wheeler, *The Journal of Chemical Physics* **69**, 3403 (1978).
- [46] J. Dudowicz, K. F. Freed, and J. F. Douglas, *The Journal of Chemical Physics* **143**, 131101 (2015).
- [47] B. Lee and G. Graziano, *Journal of the American Chemical Society* **118**, 5163 (1996).
- [48] C. Jeppesen and K. Kremer, *Europhysics Letters (EPL)* **34**, 563 (1996).
- [49] E. W. Martin, A. S. Holehouse, I. Peran, M. Farag, J. J. Incicco, A. Bremer, C. R. Grace, A. Soranno, R. V. Pappu, and T. Mittag, *Science* **367**, 694 (2020).
- [50] G. Raos and G. Allegra, *The Journal of Chemical Physics* **107**, 6479 (1997).
- [51] A. Z. Panagiotopoulos, V. Wong, and M. A. Floriano, *Macromolecules* **31**, 912 (1998).
- [52] Q. Zhang and R. Hoogenboom, *Progress in Polymer Science* **48**, 122 (2015).
- [53] A. Arsiccio and J.-E. Shea, *The Journal of Physical Chemistry B* **125**, 5222 (2021).
- [54] L. J. Abbott and M. J. Stevens, *The Journal of Chemical Physics* **143**, 244901 (2015).
- [55] S. Dhamankar and M. A. Webb, *Journal of Polymer Science* **59**, 2613 (2021).
- [56] R. B. Potts, *Mathematical Proceedings of the Cambridge Philosophical Society* **48**, 106 (1952).
- [57] J. S. Walker and C. A. Vause, *Physics Letters A* **79**, 421 (1980).
- [58] S. A. Deshmukh, S. K. R. S. Sankaranarayanan, K. Suthar, and D. C. Mancini, *The Journal of Physical Chemistry B* **116**, 2651 (2012).
- [59] C. R. Martinez and B. L. Iverson, *Chemical Science* **3**, 2191 (2012).
- [60] S. P. O. Danielsen, A. N. Semenov, and M. Rubinstein, *Macromolecules* **56**, 5661 (2023).
- [61] R. Wang and Z.-G. Wang, *Macromolecules* **47**, 4094 (2014).
- [62] A. R. Shultz and P. J. Flory, *Journal of the American Chemical Society* **74**, 4760 (1952).
- [63] Y. C. Bae, J. J. Shim, D. S. Soane, and J. M. Prausnitz, *Journal of Applied Polymer Science* **47**, 1193 (1993).
- [64] M. Arlt, W., P. M. E. A. Rasmussen, and J. M. Sorensen, *DECHEMA Chemistry Data Series, Volume V* **86**, 761 (1979).
- [65] S. Y. Oh, H. E. Yang, and Y. C. Bae, *Macromolecular Research* **21**, 921 (2013).
- [66] N. Hansen and A. Ostermeier, *Evolutionary Computation* **9**, 159 (2001).
- [67] J. Jin, A. J. Pak, A. E. P. Durumeric, T. D. Loose, and G. A. Voth, *Journal of Chemical Theory and Computation* **18**, 5759 (2022).
- [68] W. G. Noid, *The Journal of Physical Chemistry B* **127**, 4174 (2023).
- [69] S. Rekhi, D. Sundaravadivelu Devarajan, M. P. Howard, Y. C. Kim, A. Nikoubashman, and J. Mittal, *The Journal of Physical Chemistry B* **127**, 3829 (2023).
- [70] G. M. Wadsworth, W. J. Zahurancik, X. Zeng, P. Pullara, L. B. Lai, V. Sidharthan, R. V. Pappu, V. Gopalan, and P. R. Banerjee, *Nature Chemistry* **15**, 1693 (2023).
- [71] Y. An, M. A. Webb, and W. M. Jacobs, *Science Advances* **10** (2024), 10.1126/sciadv.adj2448.